

Electron energy loss spectroscopy techniques for the study of microbial chromium(VI) reduction

Tyrone L. Daulton^a, Brenda J. Little^{b,*}, Kristine Lowe^c, Joanne Jones-Meehan^c

^aMarine Geosciences Division, Naval Research Laboratory, Stennis Space Center, MS, 39529 USA

^bOceanography Division, Naval Research Laboratory, Stennis Space Center, MS, 39529 USA

^cChemistry Division, Naval Research Laboratory, Washington, DC, 20375 USA

Received 20 September 2001; received in revised form 2 January 2002; accepted 2 January 2002

Abstract

Electron energy loss spectroscopy (EELS) techniques were used to determine oxidation state, at high spatial resolution, of chromium associated with the metal-reducing bacteria, *Shewanella oneidensis*, in anaerobic cultures containing Cr(VI)O_4^{2-} . These techniques were applied to fixed cells examined in thin section by conventional transmission electron microscopy (TEM) as well as unfixed, hydrated bacteria examined by environmental cell (EC)-TEM. Two distinct populations of bacteria were observed by TEM: bacteria exhibiting low image contrast and bacteria exhibiting high contrast in their cell membrane (or boundary) structure which was often encrusted with high-contrast precipitates. Measurements by EELS demonstrated that cell boundaries became saturated with low concentrations of Cr and the precipitates encrusting bacterial cells contained a reduced form of Cr in oxidation state +3 or lower. Published by Elsevier Science B.V.

Keywords: Cr(VI); Electron energy loss spectroscopy; Environmental cell; Microbial metal reduction; *Shewanella oneidensis*; Transmission electron microscopy

1. Introduction

Chromium is a redox active 3d transition metal with a wide range (−2 to +6) of possible oxidation states of which only two are stable. Thermodynamic calculations predict hexavalent chromium, Cr(VI), is energetically favored for oxic conditions and the insoluble trivalent form, Cr(III), predominates under anoxic or suboxic conditions. Hexavalent chromium species are strong oxidants which act as carcinogens, mutagens, and teratogens in biological systems (see

Cieslak-Golonka, 1995). The structural similarity of chromate (Cr(VI)O_4^{2-}) anions (dominant Cr(VI) species at $\text{pH} < 6.1$, Brito et al., 1997) to biologically important inorganic anions, such as SO_4^{2-} and PO_4^{3-} , is likely responsible for their ability to readily transverse cell membranes, via the sulfate transport system, and be incorporated into cells (for a review see Cervantes et al., 2001). The high mobility (solubility), bioavailability (uptake), and toxicity of Cr(VI) make it a particular environmental concern.

The list of bacterial strains that tolerate or resist Cr(VI) continues to expand (for a review see Cervantes, 1991; Lovley, 1993; Fendorf et al., 2000; Wang, 2000). Several mechanisms have been proposed for microbial response to toxic metal exposure.

* Corresponding author.

E-mail address: tld@howdy.wustl.edu (T.L. Daulton).

Of these, mechanisms for Cr(VI) reduction are of particular technological and biological importance because they convert a toxic, mobile element into a less toxic, immobile form. The study of microbial Cr(VI) reduction, such as the identification of reduction intermediates, has been hindered by the lack of an analytical technique that can identify the oxidation state of chromium with subcellular spatial resolution. The most widely used method for following Cr(VI) reduction is the diphenylcarbazide colorimetric method (see Clesceri et al., 1999). Absorption at 540 nm by stoichiometric oxidation products of diphenylcarbazide reagent in acid solutions is assumed to be specific for a Cr(VI) complex. However, Cr(V), a possible intermediate in the microbial reduction process for *Pseudomonas ambigua* G-1 (Suzuki et al., 1992) and *Shewanella oneidensis* (formally classified *S. putrefaciens* MR-1) (Myers et al., 2000), also reacts with diphenylcarbazide producing a compound that absorbs at 540 nm (Eckert et al., 1991). Furthermore, hexavalent molybdenum, hexavalent vanadium, mercury and other metals, will react with diphenylcarbazide to form complexes which can contribute to the absorption at 540 nm (see Clesceri et al., 1999). Other methods used to determine oxidation state in bacteria cultures include electron spin resonance (ESR) (also called electron paramagnetic resonance (EPR) and electron magnetic resonance (EMR)) spectroscopy, and X-ray photoemission spectroscopy (XPS). Although insensitive to oxidation state, flame atomic absorption spectroscopy and inductively coupled plasma spectroscopy are routinely used to measure total chromium concentrations. All of these are bulk techniques and cannot provide detailed information on the subcellular (submicron) level necessary for understanding microbial reduction processes.

Both transmission electron microscopy (TEM) and scanning electron microscopy (SEM) have sufficient resolution to study the spatial relationship between cells and reduction products, as well as their chemistry. With electron microscopy, energy-dispersive X-ray spectroscopy (EDXS) can be used to measure the characteristic X-rays emitted when atoms in a specimen return to their ground state following core-level ionization by the electron beam. For example, EDXS has been used to identify elements present in reduction products associated with bacteria (Hill and Cowley, 1986; Fude et al., 1994; Badar et al., 2000;

McLean et al., 2000; Smith and Gadd, 2000; McLean and Beveridge, 2001) and wetland plants (Lytle et al., 1998). Although straightforward to use for elemental identification, EDXS is insensitive to oxidation state. On the other hand, electron energy loss spectroscopy (EELS), which directly measures the energy loss of incident electrons inelastically scattered from atoms in the specimen, is a direct probe of the electron configuration around atoms, and can determine the oxidation state of $3d$ and $4d$ transition metals at high spatial resolution (Krishnan, 1990; Paterson and Krivanek, 1990; Cressey et al., 1993; van Aken et al., 1998). Furthermore, EELS techniques have been used to produce oxidation state maps using energy filtered imaging (Wang et al., 1999, 2000).

Determination of oxidation state by EELS is accomplished by analyzing valence-induced differences in fine structure of L_2 and L_3 (or collectively $L_{2,3}$) absorption edges by comparison of unknowns to standards of known oxidation state. In an EELS core-loss spectrum, an absorption “edge” is a sudden increase in electron energy loss that immediately follows the threshold energy for ionization of a core electron. Edges are denoted by electronic level ionized, K, L, M, etc., following standard spectroscopic nomenclature. The $L_{2,3}$ absorption edges arise from transitions to unoccupied d levels from two spin-orbit split levels, $2p_{1/2}$ level (producing the L_2 edge) and the $2p_{3/2}$ level (producing the L_3 edge). The valence of a transition metal is related to the number of holes in the d level, (i.e., the $3d^n$ or $4d^n$) configuration. For example, tetrahedral Cr(VI) has an empty d orbital ($3d^0$ configuration) and octahedral Cr(III) has a $3d^3$ configuration. Since $L_{2,3}$ absorption edges are inherently dependent on the number of unoccupied d levels in $3d$ and $4d$ transition metals, they are sensitive to valence state.

In general, oxidation state can affect the position, shape and relative intensity of $L_{2,3}$ absorption edges. Techniques used to determine mixed/single valence states involve analysis of the following: (a) the position of the $L_{2,3}$ absorption edges, which depends on the screening of the nuclear field of a metal atom by the presence of valence-electron charge; absorption edges generally shift to higher energy with increased oxidation state, (b) the ratio of the $I(L_3)/I(L_2)$ integrated-peak intensity (henceforth abbreviated as L_3/L_2) which depends on the number of electrons in the

final (4d or 4f) state; white-line ratios generally decrease with increased oxidation state (e.g., van Aken et al., 1998), and (c) least squares fits of summed spectra of standards or calculations to the shape of $L_{2,3}$ absorption edges (e.g., Cressey et al., 1993). Furthermore, the total $L_{2,3}$ absorption edge (or white line) intensity, normalized to the post L-edge continuum, has been used to determine the *d*-electron occupancies in transition metals (e.g., Pearson et al., 1993). However, L_3/L_2 peak ratios are more sensitive to valence state than the normalized white line intensities as shown by energy-filtered imaging (Wang et al., 1999).

The application of TEM EELS techniques to actual microcharacterization of mineral oxidation state has been underutilized because of the difficulties in applying the techniques. For example, despite the detailed, submicron-scale information they can provide, to our knowledge, EELS techniques have never been applied in microbial reduction studies. In fact, previous TEM studies only assume microbial Cr(VI) reduction products are Cr(III) (e.g., McLean et al., 2000; McLean and Beveridge, 2001). Although this assumption is likely correct, since Cr(III) is a stable and insoluble reduced form, the oxidation state of the Cr associated with bacteria has not yet been determined by direct measurement.

The purpose of this paper is to demonstrate the application of EELS techniques for the determination of oxidation state of metals associated with bacteria. A description of methods for collecting EELS spectra, selection of standards, spectra analysis, and data interpretation are discussed. In particular, Cr(VI) reduction by *S. oneidensis* (previously *S. putrefaciens* strain MR-1; Venkateswaran et al., 1999) was studied.

2. Cultures, methods, and techniques

2.1. Cultures

S. oneidensis (Venkateswaran et al., 1999), previously classified *S. putrefaciens* strain MR-1 (MacDonell and Colwell, 1985), and as *Alteromonas putrefaciens* (Lee et al., 1977), was isolated from the anaerobic zone of Mn-rich sediments in Oneida Lake, NY (Myers and Nealson, 1988b). *S. oneidensis* is a Gram-negative, facultative bacterium, capable of

respiring aerobically and anaerobically using a variety of terminal electron acceptors, including: Fe(III), Mn(IV), NO_2^- , NO_3^- , SO_2 , sulfite (SO_3^{2-}), thio-sulfate ($\text{S}_2\text{O}_3^{2-}$), tetrathionate ($\text{S}_4\text{O}_6^{2-}$), trimethylamine *N*-oxide, fumarate, glycine, Cr(VI), U(VI), and Tc(VII) (see Myers and Nealson, 1988a,b; Lovley et al., 1991; Lloyd and Macaskie, 1996). The bacteria were initially grown under aerobic conditions at 30 °C for 18 to 24 h in Luria–Bertani (LB) broth (Difco Laboratories, Detroit, MI, USA) with continuous agitation. An aliquot (5 ml) of the initial culture was transferred to flasks containing 250 ml of an anaerobic growth medium (adapted from Myers and Nealson, 1988a). The growth medium consisted of autoclaved $d\text{H}_2\text{O}$, a salt component (9.0 mM $(\text{NH}_4)_2\text{SO}_4$, 5.7 mM $\text{K}_2\text{HPO}_4 \cdot 3\text{H}_2\text{O}$, 3.3 mM KH_2PO_4 , and 2.0 mM NaHCO_3), and a trace metal component (70 μM $\text{Na}_2\text{EDTA} \cdot 2\text{H}_2\text{O}$, 60 μM H_3BO_3 , 10 μM NaCl , 6 μM $\text{FeSO}_4 \cdot 7\text{H}_2\text{O}$, 5 μM $\text{CoCl}_2 \cdot 6\text{H}_2\text{O}$, 5 μM $\text{Ni}(\text{NH}_4)(\text{SO}_4)_2 \cdot 6\text{H}_2\text{O}$, 4.0 μM $\text{Na}_2\text{MoO}_4 \cdot 2\text{H}_2\text{O}$, 1.5 μM Na_2SeO_4 (anhyd), 1.3 μM $\text{MnSO}_4 \cdot \text{H}_2\text{O}$, 1.0 μM $\text{ZnSO}_4 \cdot 7\text{H}_2\text{O}$, and 0.2 μM $\text{CuSO}_4 \cdot 5\text{H}_2\text{O}$). The following amino acids and vitamins were present in the medium: 10^{-4} mg l^{-1} casamino acids, 10^{-3} mg l^{-1} vitamin B₁ (Thiamine), 0.02 mg l^{-1} L-arginine HCl, 0.02 mg l^{-1} L-glutamic acid, 0.02 mg l^{-1} L-glutamine, and 0.04 mg l^{-1} L-serine. The following co-factors were present in the medium: 1 mM $\text{MgSO}_4 \cdot 7\text{H}_2\text{O}$ and 0.5 mM $\text{CaCl}_2 \cdot 2\text{H}_2\text{O}$. The carbon source was sodium lactate (18 mM).

For reduction rate experiments, cells were grown to an optical density of 0.5 (at 600 nm), approximately 10^8 cells cm^{-3} . Five experimental runs were performed: live resting cells, cell-free supernatant, sodium azide-treated cells (to inhibit respiration), heat-treated cells (to terminate metabolic and reductase functions), and sterilized cell-free media. Live cells were treated with antibiotic chloramphenicol (final concentration = 100 $\mu\text{g}/\text{ml}$) to inhibit protein synthesis, stop cell division, and maintain a constant cell population. The second culture of cells was treated with 1% sodium azide for 15 min. Cells were centrifuged at 10⁴ rpm for 10 min (supernatant discarded), washed with sterile 1 × phosphate-buffered saline, centrifuged, and resuspended in LB media. The third culture of cells was heat-treated in a 60 °C water bath for 15 min with periodic shaking. In all reduction rate experiments, K_2CrO_4 was added to the anaerobic medium to a con-

centration of $100 \mu\text{M}$ of CrO_4^{2-} , to serve as an electron acceptor. The cultures were purged with N_2 for 20 min with out-gassing to remove dissolved O_2 . Samples were periodically removed and Cr concentration was estimated using the diphenylcarbazide method.

For conventional TEM studies, cells were grown anaerobically in the defined medium with K_2CrO_4 (concentration of $100 \mu\text{M}$ CrO_4^{2-}). Cultures were incubated at room temperature on a bench-top stir plate attached to a N_2 gas line for 30 days. Samples (1 ml) from the 30-day culture were pelleted by centrifugation (1 min at 10^4 rpm), and fixed in 1 ml, 5% aqueous solution of glutaraldehyde (Grade I, Sigma) overnight at room temperature. Fixed cells were washed three times in distilled water, and treated with 2% osmium tetroxide (aqueous solution) for 1 h. After washing three times in distilled water, the pellets were processed through a gradual ethanol dehydration sequence (in 35%, 50%, 75%, then 95% ethanol in deionized water), three 10-min washes in 100% ethanol, and three 10 min washes in propylene oxide. The specimen was embedded in Spurr's resin (Spurr, 1969) for its low viscosity. Increasing concentrations of Spurr's resin in propylene oxide were infiltrated into the pellets at mixtures of 1:1, 2:1, 3:1 and 100% resin for 1 h each. Cell pellets were infiltrated again with fresh Spurr's resin for 1 h and cured at 70° for 2 days. Specimens of 80 nm thickness were sectioned from the embedded blocks using a Leica UltraCut UCT microtome and mounted on amorphous carbon (a-C) coated Cu TEM grids.

For environmental cell (EC)-TEM studies, cells were grown anaerobically in the defined medium with K_2CrO_4 ($100 \mu\text{M}$ CrO_4^{2-}). Initial pH was approximately 6.7. Cultures were incubated at room temperature on a bench-top stir plate attached to a N_2 gas line. The culture was aseptically sampled and analyzed for Cr(VI) concentration using the diphenylcarbazide method during the course of the incubation. The culture was spiked with K_2CrO_4 after 96, 120, 144, 168, 408, 672, 840, 1008, and 1128 h. A total of 0.275 mol K_2CrO_4 was added to the culture. After a 51-day incubation, 200 ml of culture were removed from the flask, sealed in a test tube, and shipped for EC-TEM examination. Bacteria were examined 53 days after inoculation. In contrast to conventionally prepared TEM specimens, EC-TEM specimen preparation was minimal. The sample was centrifuged,

supernatant removed, and the pellet rinsed with distilled water to remove trace salts. An aliquot (several microliters) containing suspended bacteria was quickly loaded into the EC-specimen holder and examined under an atmosphere at 100 Torr of air saturated with water vapor.

2.2. Transmission electron microscopy

A JEOL JEM-3010 transmission electron microscope operating at 300 keV with a LaB_6 filament was used in this study. This instrument is equipped with an EDXS system, a Gatan imaging filter (GIF200) capable of EELS, and a JEOL EC system with two interchangeable EC-specimen holders. Both in-situ EC-TEM specimen holders are capable of circulating dry or water-saturated gas at flow rates of 0–15 Torr min^{-1} through the specimen chamber at 10^{-3} to 250 Torr pressure. The EC-TEM system is of the closed cell type (Fukami et al., 1991), and confinement of the pressurized environment within the EC is achieved with electron-transparent, a-C with the specimen supported on the lower EC window.

2.3. EELS techniques for oxidation state determination

In this study, two EELS techniques were used to identify oxidation state of Cr associated with bacteria. Oxidation state is determined by both the chemical shift of $L_{2,3}$ edges and the ratio of L_3/L_2 , integrated-peak intensities, the two most sensitive and straightforward techniques. Results of both techniques are used here, in combination, to yield higher confidence (and accuracy) of the oxidation state determination. In contrast, previous EELS studies have focused on demonstrating the capability of one technique, rather than applying techniques in combination to actual microcharacterization in physical systems.

In the first technique, L_3 edges are more suitable for measuring chemical shift than L_2 edges because their intrinsic line widths are narrower and better defined. The extra broadening of the L_2 threshold peak results from the shorter lifetime of the excited state associated with L_2 which can decay by an extra Coster–Kronig Auger decay channel not available for the excited state associated with the L_3 edge (e.g., see Zaanen and Sawatzky, 1986). The chemical

shift technique is more straightforward, and previously published results on well-characterized standards can be readily used. However, this technique cannot be used for quantitative determination of mixed oxidation states because the shift in absorption edges is small (e.g., ≈ 2 eV between Cr(VI) and Cr(III)) in comparison to typical peak widths (i.e., EELS resolution). The L_3/L_2 intensity ratio technique can be quantitatively applied to materials with mixed oxidation states. However, it is sensitive to analysis conditions such as the subtraction of background intensity due to transitions to unoccupied states in the continuum, as well as peak integration widths. These details can vary among researchers. Since it is necessary to analyze standards and unknowns using identical procedures, published L_3/L_2 peak ratio results are of limited use. Furthermore, in the selection of oxidation state standards it is important that the standards are not sensitive to electron beam damage where they could change oxidation state in addition to crystal structure and/or composition.

2.4. EELS experimental parameters

The following conditions were used during collection of EELS spectra under EC-TEM and TEM conditions: an illumination angle $2\alpha = 4\text{--}10$ mrad, a collection angle of $2\beta = 10.8$ mrad, a 2-mm entrance aperture, and an energy dispersion of 0.1 eV/channel. Low-loss spectra were acquired with an integration time of 0.128 s and core-loss spectra between 0.512 and 1.02 s. For each acquisition, 10 (EC-TEM) or 25 (conventional TEM) spectra were summed. Spectra were collected in diffraction mode of the transmission electron microscope (i.e., image coupling to the EELS spectrometer) and were corrected for dark current and channel-to-channel gain variation of the charge coupled device (CCD) detector.

Energy calibration of the core-loss regime and measurement of energy drift during data acquisition were performed by collecting zero-loss spectra before and following collection of core-loss spectra. Energy of core-loss spectra was calibrated using the average position of the two zero-loss peaks. The error in the energy calibration corresponded to the energy drift of the zero-loss peaks. In addition, a C–K edge spectrum was acquired immediately following spectrum collection from the O–K/Cr–L core-loss regime. The

position of the C–K ($1s$) peak at 284.9 eV (arising from transitions to the π^* molecular orbital) from the TEM a-C support film was used to evaluate the energy calibration. Only sets of spectra whose energy calibration was consistent with the position of the C–K, π^* peak were used. Either the pre-O–K edge background or the pre-Cr–L edge background (depending on the analysis to be performed) was subtracted from core-loss spectra using a power law and plural inelastic scattering was removed by Fourier deconvolution methods (Egerton, 1996).

Chromium standards were analyzed by conventional TEM. Standards were produced by placing high purity Cr(II)F₂, Cr(II)Se, Cr(III)Cl₃, Cr(III)₂O₃, KCr(III)(SO₄)₂·12H₂O, and K₂Cr(VI)O₄ powders directly on Cu TEM grids coated with holey a-C. Once the standard was prepared, it was examined immediately. For each standard, 20 individual grains were analyzed by EELS. Results were averaged and the errors reported for the mean represent the standard error of those measurements.

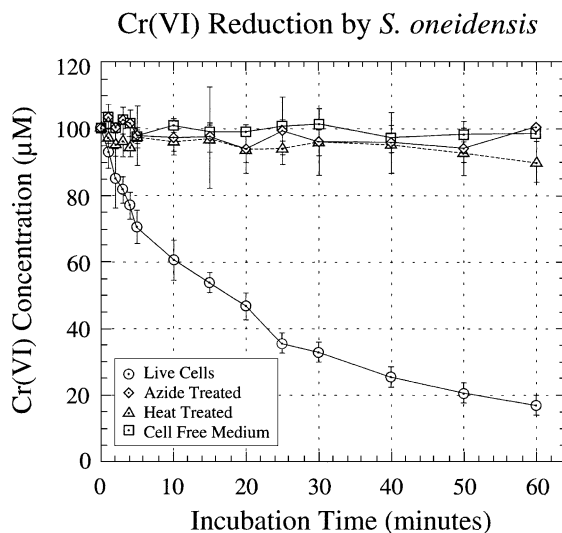


Fig. 1. Relative rates of Cr(VI) reduction in *S. oneidensis*-inoculated, antibiotic chloramphenicol-treated (cell division inhibitor to maintain a constant cell population), sodium azide-treated (respiratory inhibitor), and heat-treated (to terminate cell metabolic activity) cultures. A colorimetric assay using spectrophotometry was used to measure Cr(VI) concentration. To guide the eye, data points are connected by straight lines, and a dotted line is used to differentiate two close data sets.

3. Results

3.1. Reduction rate experiments

To establish that respiring cells were responsible for the reduction of Cr(VI), the reduction rate of live, resting cells of *S. oneidensis* were compared to cell-free supernatants, sodium azide-treated bacteria (to inhibit respiration), heat-treated bacteria (to terminate metabolic and reductase activity), and sterile (cell-free) medium. The concentration of Cr(VI) in cultures was periodically measured using the diphenylcarbazide colorimetric assay (Fig. 1). Each data point represents

the average of three measurements and the error bars represent the standard error of the mean. Live, resting cells of *S. oneidensis* reduced approximately 80% of 100 μM Cr(VI) in 1 h. In comparison, no significant Cr(VI) reduction occurred in cell-free supernatants (data not shown), azide-treated cells, heat-treated cells, and sterile (abiotic) medium controls (Fig. 1).

3.2. Direct imaging

Examination of *S. oneidensis* by EC-TEM at 100 Torr, under a circulation of air saturated with water vapor (2 Torr min^{-1}), showed the rod-shaped

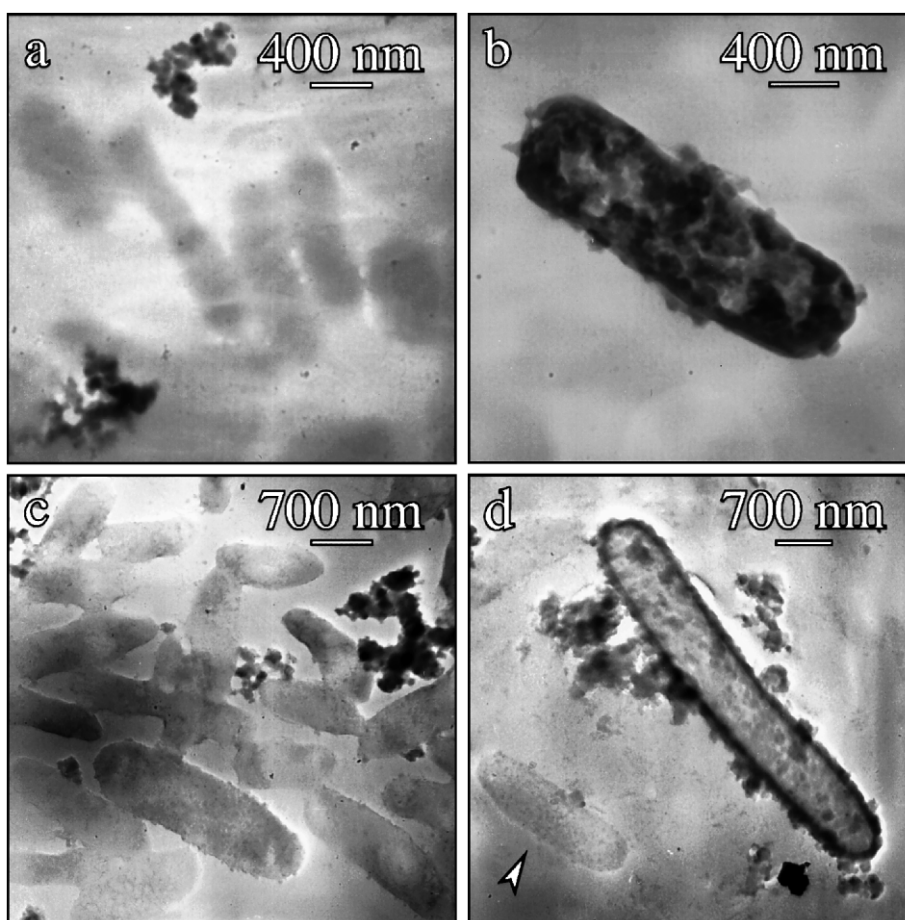


Fig. 2. *S. oneidensis* imaged by EC-TEM at 100 Torr: (a, c) bacteria exhibiting low contrast in bright-field imaging and (b, d) bacteria encrusted/impregnated with electron dense particulate. The arrowhead in panel (d) points to a low-contrast bacterium in the same field of view as a bacterium with electron dense particulate, illustrating the dramatic contrast difference. The low-contrast, diffuse background, best seen in panel (a), represents the extracellular polymeric substances that surround the cells.

morphology typical of the species (Fig. 2). The micrographs demonstrate that bacterial membranes were intact and did not show evidence of rupture from partial decompression. Cells remain plump/hydrated while extracellular polymers surrounding the cells retain moisture. In comparison, unfixed cells deposited on a holy a-C film and examined under high vacuum by conventional TEM (not shown), exhibit ruptured cell membranes, as well as loss of both cell and extracellular polymer mass through dehydration.

Direct imaging reveals two distinct populations of *S. oneidensis* in the cultures: bacteria exhibiting low image contrast (Fig. 2a,c) and bacteria exhibiting electron dense, high-contrast cell boundaries often encrusted with high-contrast precipitates (Fig. 2b,d). Cross-sectional images of bacteria by conventional TEM (Fig. 3) show no evidence of intracellular precipitates, suggesting precipitates are restricted to the outer surface of the bacteria. Precipitates ranged in size between ≈ 10 and 200 nm, and selected area diffraction indicated that the grains were predominantly amorphous perhaps due to a high degree of hydration. Often the cells exhibited a 30- to 49-nm

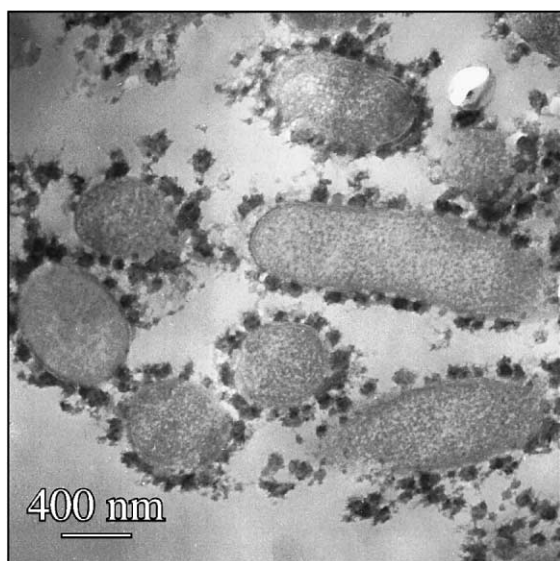


Fig. 3. *S. oneidensis* imaged by conventional TEM in ≈ 80 -nm thick, thin section. The field of view displays several bacterial cells in random, oblique cross-section. Cross-sectional images show precipitates occur on the outer cell surface and no evidence of intracellular precipitates is observed.

thick, high-contrast perimeter, indicating that the cell boundary became saturated with absorbed elements of heavy mass.

3.3. Chemical analysis by EELS

Fig. 4 shows EELS low-loss and core-loss spectra collected from an encrusted bacterium examined by EC-TEM. The dominant feature in the low-loss spectrum is the zero-loss peak corresponding to electrons that escaped inelastic collisions. The width of the zero-loss peak is a measure of the energy distribution of the incident beam and corresponds to the best energy resolution of the spectrometer (energy resolution typically decreases with increasing energy loss). The narrow zero-loss peak (Fig. 4) shows energy resolution is not significantly affected by transmission through the hydrated, pressurized environment of the EC. The broad feature around 25 eV in the low-loss spectrum corresponds to plasmon excitations (i.e., collective excitations of valence electrons). The ratio of the integrated intensity under the zero-loss and plasmon peaks is related to specimen thickness. The relative height of the two peaks illustrates that multiple scattering is not severe in the EC. The total thickness traversed by the electron beam, estimated by the log-ratio technique (Egerton, 1996), is 1.13λ , where λ is the total mean free path for inelastic scattering through the EC windows and specimen. The low-loss spectrum also exhibits a sharp feature at 13.2 eV that is only observed in EELS spectra collected in the EC. It is consistent with the EELS K-edge of hydrogen (Geiger and Schmoranzler, 1969), which can be produced by electron beam radiolysis of water in the hydrated specimen. For example, similar EELS edges at 13 eV have also been observed concurrently with electron beam-induced bubble formation from frozen-hydrated biological specimens and attributed to hydrogen formation (Leapman and Sun, 1995).

In the core-loss spectrum of encrusted *S. oneidensis* examined by EC-TEM, a strong O–K edge signal produced by O 1s transitions was observed at 537.1 ± 0.5 eV due to H₂O in the hydrated bacterium and extracellular substances. A less intense feature at 529.2 ± 0.5 eV can be attributed to oxygen 2p hybridization with the Cr 3d band, while the broad feature at 558 eV can be attributed to plural (O–K core-loss

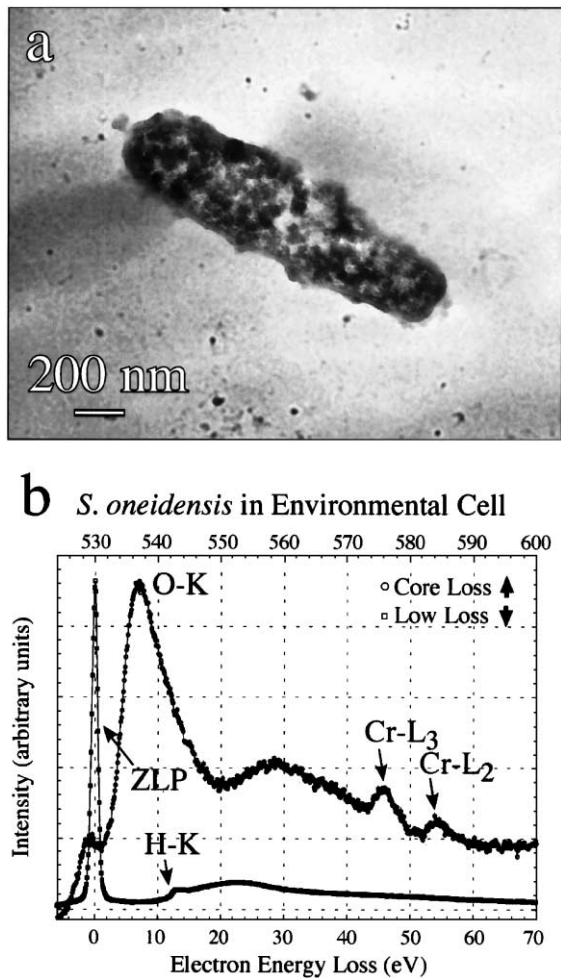


Fig. 4. *S. oneidensis* imaged by EC-TEM at 100 Torr: (a) cell is encrusted with electron dense particulate. (b) EC-TEM EELS spectrum from the bacterium demonstrates the presence of Cr. Both the low-loss spectrum containing the zero-loss peak (ZLP) and the core-loss spectrum of the O–K and Cr–L absorption edges are shown. The ZLP represents electrons that have undergone elastic and quasi-elastic (mainly phonon) interactions. Its full width at half maximum is a measure of the instrumental resolution, which under these EC-TEM conditions is ≈ 1 eV. The top abscissa corresponds to the low-loss spectrum and the bottom abscissa corresponds to the core-loss spectrum.

plus plasmon) scattering. The presence of Cr is clearly shown by the characteristic pair of Cr–L₂ and Cr–L₃ edges in the EELS spectrum indicating that the precipitates are Cr-rich.

Bacterial cultures were also examined in cross-section by conventional TEM. Spectra collected from

individual precipitates encrusting the outer cell boundary of *S. oneidensis* (Fig. 5) showed characteristic Cr–L_{2,3} edges. The sectioned precipitates selected for analysis were those loosely attached to the bacterial outer surface where spectra could be collected without contributions from the bacteria. In addition, the electron-dense cell boundary of *S. oneidensis* cells that lacked precipitates encrusting the surface was examined by EELS in cross-section. Spectra from the cell boundary revealed characteristic Cr–L_{2,3} edges indi-

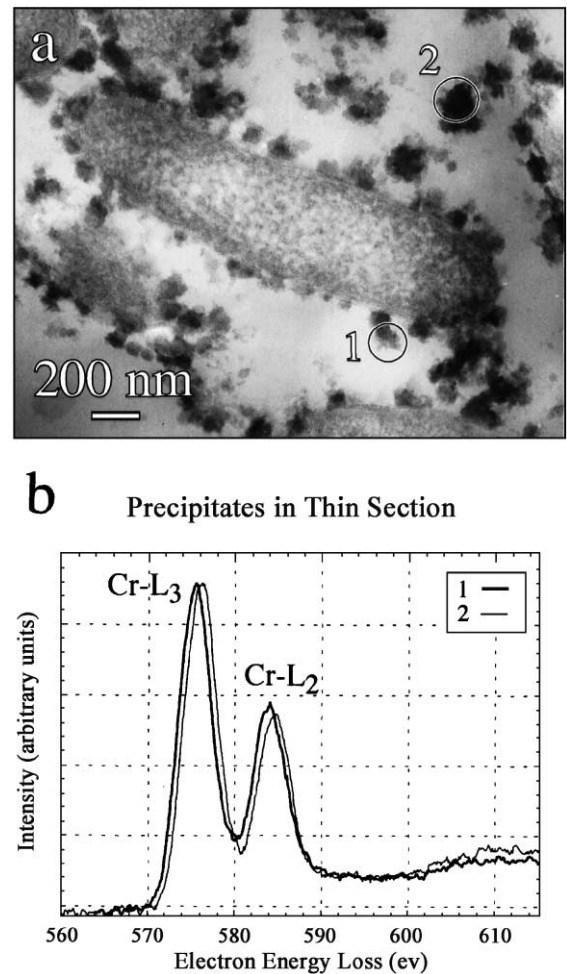


Fig. 5. *S. oneidensis* imaged by conventional TEM in ≈ 80 -nm thick, thin section: (a) cell is encrusted with electron dense particulate; (b) EELS spectra from the isolated precipitates demonstrates the presence of Cr. The particulates analyzed are labeled and the diameter of the circle corresponds to the electron probe diameter.

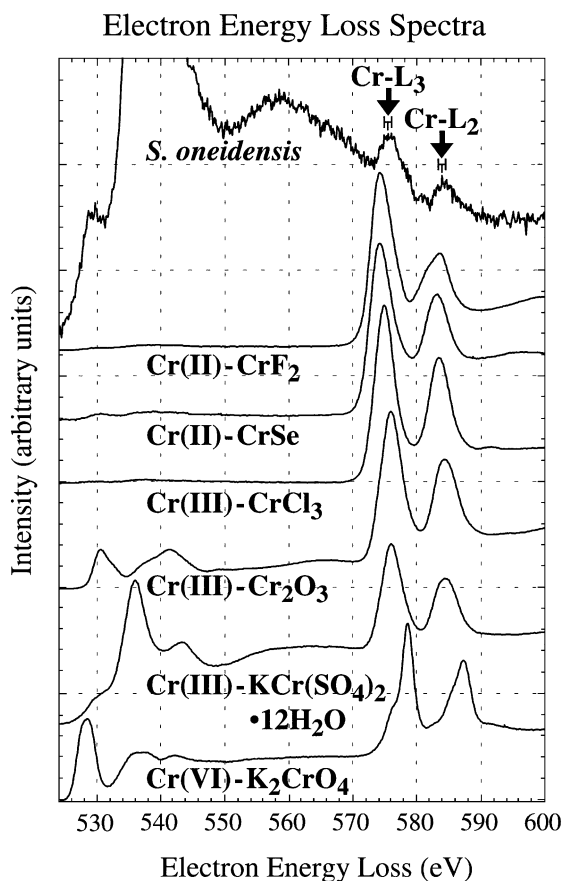


Fig. 6. A comparison of the core-loss EELS spectra of encrusted *S. oneidensis* in the EC at 100 Torr and Cr standards of known oxidation state. Spectra were normalized to the intensity of the L_3 peak and offset from one another. The spectra shown for the Cr standards represent the sum of 20 individual spectra acquired. The error bars shown for *S. oneidensis* represent the error in energy loss calibration for that spectrum only. For the errors associated with the other spectra, see Table 1.

cating the cell boundary was saturated with absorbed Cr at concentrations likely too low to be detected by EDXS; EELS has higher sensitivity than EDXS.

A comparison of core-loss spectra from encrusted, hydrated *S. oneidensis* (collected by EC-TEM) and Cr standards of known oxidation state (collected by conventional TEM) is shown in Fig. 6. The spectrum of $\text{KCr}(\text{SO}_4)_2 \cdot 12\text{H}_2\text{O}$ exhibited a peak at 535.7 eV similar to the stronger feature observed in the spectrum from hydrated *S. oneidensis*, and likely corresponds to H_2O bound in the structure. More impor-

tantly, systematic differences in Cr- $L_{2,3}$ fine structure are apparent in the spectra of standards (Fig. 6). For example, the Cr- $L_{2,3}$ lines for the standards show a systematic shift in edge-peak energy and variation in relative intensity with oxidation state (Fig. 6). In addition, the Cr- $L_{2,3}$ lines of the K_2CrO_4 peaks are further differentiated in that they appear asymmetric because each is split into two separate peaks separated by ~ 2 eV.

3.4. EELS oxidation state analysis of standards

Oxidation state was identified by both the L_3 peak positions and the ratio of L_3/L_2 integrated-peak intensities. Measurement of the L_3 peak positions is straightforward and the results for Cr standards are shown in Fig. 7 and summarized in Table 1. For measurement of the ratio of L_3/L_2 integrated-peak intensities, two methods of background subtraction were used. The first method, illustrated in Fig. 8, is similar to the double step function used by Pearson et al. (1993). In this method, the Cr- L_3 pre-absorption edge was fit to a power law and subtracted. A linear function was then fit to the Cr- L_2 post-edge region over a 20-eV window (extending from 600 to 620 eV). Typically, background windows are chosen

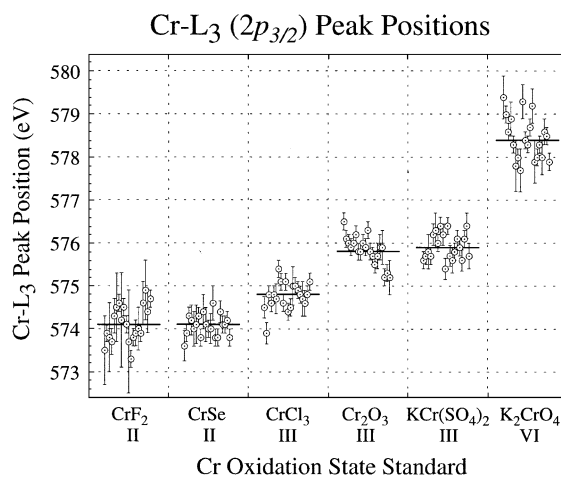


Fig. 7. The measured L_3 peak positions for the Cr oxidation-state standards. The error bars for the data points represent the measured drift in the EELS spectrometer during acquisition. The bar represents the mean of the measured values. Roman numerals along the abscissa indicate the formal valence state of Cr in the standard.

Table 1
Cr–L₃ (2p_{3/2}) and Cr–L₂ (2p_{1/2}) adsorption edges

XPS—binding energies, EELS—L-edge peak positions					
Compound	Formal Valence	Cr–L ₃ (2p _{3/2}) (eV)	Cr–L ₂ (2p _{1/2}) (eV)	Technique	Refs.
Cr	0	573.8	583.0	XPS	Allen and Tucker, 1976
		574.1		XPS	Moffat et al., 1995
		574.1	583.5	XPS	Asami and Hashimoto, 1977
		574.3 ^a	582.8 ^a	EELS	Fink et al., 1985 ^a
		576.5 ± 1.0	585.0 ± 1.0	EELS	Leapman et al., 1982 ^b
CrP	0	574.2		XPS	Moffat et al., 1995
Cr(CO) ₆	0	577.6	586.3	XPS	Allen and Tucker, 1976
CrF ₂	II	574.2 ± 0.1	583.5 ± 0.1	EELS	This study
CrSe	II	574.2 ± 0.1	583.1 ± 0.1	EELS	This study
CrCl ₃	III	574.9 ± 0.1	583.4 ± 0.1	EELS	This study
		576.4	587.4	XPS	Allen and Tucker, 1976
CuCrO ₂	III	576.4 ± 0.2	586.2 ± 0.2	XPS	Allen et al., 1973 ^c , Allen and Tucker, 1976
NaCrO ₂	III	577.0 ± 0.2	586.9 ± 0.2	XPS	Allen et al., 1973 ^c , Allen and Tucker, 1976
Cr ₂ O ₃	III	575.9 ± 0.1	584.3 ± 0.1	EELS	This study
		576.5	586.0	XPS	Asami and Hashimoto, 1977
		576.6–576.8		XPS	Moffat et al., 1995
		576.8 ± 0.2	586.2 ± 0.2	XPS	Allen et al., 1973 ^c , Allen and Tucker, 1976
		576.8	584.8	EELS	Krivanek and Paterson, 1990
		576.8	586.7	XPS	Ikemoto et al., 1976
		577.9 ± 1.0	585.8 ± 1.0	EELS	Leapman et al., 1982 ^b
FeCr ₂ O ₄	III	576.0	584.0	XPS	Kendelewicz et al., 1999
KCr(SO ₄) ₂ ·12H ₂ O	III	576.0 ± 0.1	584.5 ± 0.1	EELS	This study
		581.0	590.5	XPS	Allen et al., 1973 ^c , Allen and Tucker, 1976
LaCrO ₃	III	576.1 ± 0.09	585.8 ± 0.05	XPS	Konno et al., 1992
LiCrO ₂	III	577.0 ± 0.2	586.8 ± 0.2	XPS	Allen et al., 1973 ^c , Allen and Tucker, 1976
CrOOH	III	577.0	586.9	XPS	Ikemoto et al., 1976
Cr(OH) ₃ ·0.4H ₂ O	III	577.0	586.4	XPS	Asami and Hashimoto, 1977
		577.1		XPS	Moffat et al., 1995
CrP	III	577.4		XPS	Moffat et al., 1995
CrCl ₃ ·6H ₂ O	III	577.5		XPS	Moffat et al., 1995
CrPO ₄	III	577.8		XPS	Moffat et al., 1995
CrBO ₃	III	578.0		XPS	Moffat et al., 1995
Cr ₂ (SO ₄) ₂ ·15H ₂ O	III	578.6		XPS	Moffat et al., 1995
CrO ₂	IV	576.3	586.0	XPS	Ikemoto et al., 1976
LaCrO ₄	V	578.8 ± 0.21	588.0 ± 0.22	XPS	Konno et al., 1992
CrO ₃	VI	578.3 ± 0.2	587.0 ± 0.2	XPS	Allen et al., 1973 ^c
		579.1	588.3	XPS	Asami and Hashimoto, 1977
CaCrO ₄	VI	578.9 ± 0.2	588.1 ± 0.2	XPS	Allen et al., 1973 ^c , Allen and Tucker, 1976
BaCrO ₄	VI	579.1 ± 0.2	588.4 ± 0.2	XPS	Allen et al., 1973 ^c , Allen and Tucker, 1976
K ₂ Cr ₂ O ₇	VI	579.4 ± 0.2	588.8 ± 0.2	XPS	Allen et al., 1973 ^c , Allen and Tucker, 1976
		579.8	589.1	XPS	Ikemoto et al., 1976
Na ₂ Cr ₂ O ₇	VI	579.4 ± 0.2	588.5 ± 0.2	XPS	Allen et al., 1973 ^c , Allen and Tucker, 1976
Rb ₂ Cr ₂ O ₇	VI	579.4 ± 0.2	588.7 ± 0.2	XPS	Allen et al., 1973 ^c , Allen and Tucker, 1976
Cs ₂ Cr ₂ O ₇	VI	579.5 ± 0.2	588.7 ± 0.2	XPS	Allen et al., 1973 ^c , Allen and Tucker, 1976
SrCrO ₄	VI	579.6 ± 0.2	588.6 ± 0.2	XPS	Allen et al., 1973 ^c , Allen and Tucker, 1976
K ₂ CrO ₄	VI	578.6 ± 0.1	587.2 ± 0.1	EELS	This study
		579.6 ± 0.2	588.9 ± 0.2	XPS	Allen et al., 1973 ^c , Allen and Tucker, 1976
PbCrO ₄	VI	578.6	587.2	XPS	Kendelewicz et al., 1999
		580.9	587.8–589.5	EELS	Brydson et al., 1993
Cs ₂ CrO ₄	VI	579.8 ± 0.2	588.8 ± 0.2	XPS	Allen et al., 1973 ^c , Allen and Tucker, 1976
Li ₂ CrO ₄	VI	579.8 ± 0.2	589.0 ± 0.2	XPS	Allen et al., 1973 ^c , Allen and Tucker, 1976
Na ₂ CrO ₄	VI	579.8 ± 0.2	589.1 ± 0.2	XPS	Allen et al., 1973 ^c , Allen and Tucker, 1976

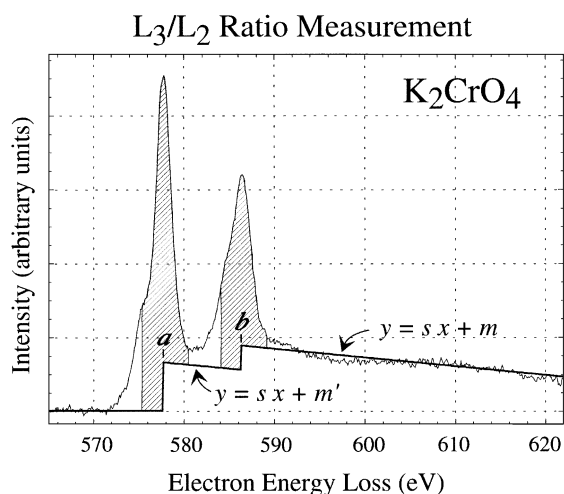


Fig. 8. Core-loss EELS spectrum for K_2CrO_4 illustrating the background subtraction used in method I. The step function (bold line) used to subtract the background from the $L_{2,3}$ edges and the areas integrated to yield peak intensities (shaded regions) are shown. The fitting parameters a , b , s , and m are: the L_3 maximum, the L_2 maximum, the slope of the linear function fitted to the 20 eV post L_2 edge region (600–620 eV), and the intercept of the linear function. The parameter m' is given by $m' = (2m - as)/3$.

between 50 and 100 eV because smaller windows are susceptible to plural scattering effects. However, there were insufficient channels in the data to use a larger window since the O–K edge region was included. The fitted background was extrapolated into the L_2 threshold region. A linear step function was inserted at the L_2 maximum and a straight line (of the same slope as that fitted to the Cr– L_2 post-edge region) was extrapolated into the L_3 threshold. A second step function was inserted at the L_3 maximum and set to zero below the L_3 maximum. The ratio for the step heights was set at 2:1, consistent with the multiplicity of the initial states, that of four $2p_{3/2}$ electrons and two $2p_{1/2}$ electrons. It should be noted that the ratios of L_3 to L_2 intensities do not follow the expected 2:1 ratio for early $3d$ transition metals (Leapman and Grunes, 1980). These anomalous ratios can be partially explained by atomic multiplet effects producing over-

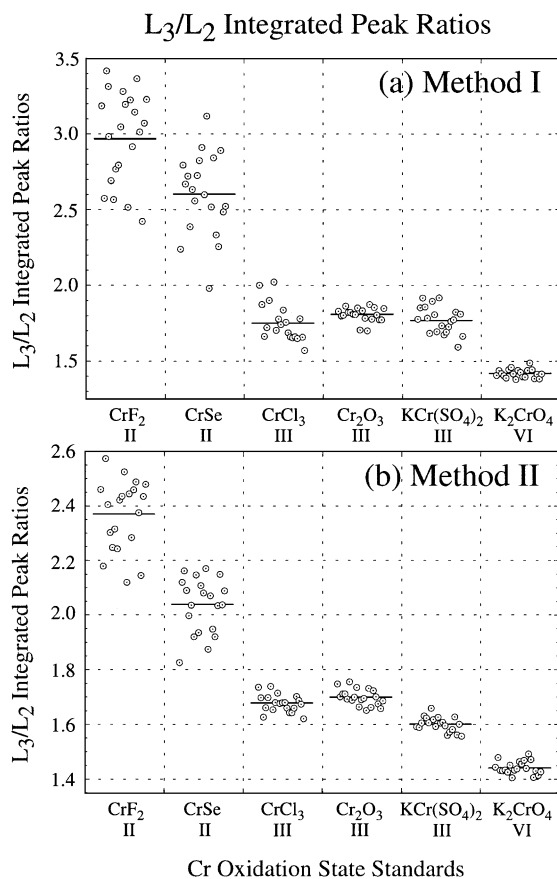


Fig. 9. The measured L_3/L_2 integrated-peak intensity ratios for the Cr oxidation-state standards: (a) background subtraction method I and (b) background subtraction method II. The bar represents the mean of the measured values. There is no straightforward method to determine experimental errors for the individual measurements so none are reported. Roman numerals along the abscissa indicate the formal valence state of Cr in the standard.

lapping transitions from $2p_{3/2}$ and $2p_{1/2}$ states (Zaanen et al., 1985). Nonetheless, an approximation of 2:1 is sufficient for this work.

Although the first subtraction method approximates the decreasing background, the fit of Cr– L_2 post-edge region was often affected by a broad post-edge feature, containing plural scattering effects

Notes to Table 1:

^a As reported in reference as binding energies.

^b EELS L-edge onsets quoted in reference, however L-peak positions are shown here.

^c After recalibrating the XPS, Au $4f_{7/2}$ line from 82.8 to 84.0 eV.

not completely removed from the spectra. The post-edge feature varied with each spectrum, introducing scatter in the L_3/L_2 peak ratio measurements. To provide a more consistent background subtraction for all spectra, a second method using a flat, two-step function was applied. The second background fitting procedure is identical to the first except the slope of the linear function is set to zero and it is fit to a 2-eV wide window immediately following the Cr– L_2 peak, in the edge tail, prior to the post-edge feature.

Once the background was subtracted using either of the two methods, the Cr–L peaks were integrated over a 5 eV window. The L_3/L_2 peak ratios for the Cr standards are shown in Fig. 9 and summarized in Table 2. The flat, two-step background subtraction method yielded lower values, however, less relative scatter in the data. The core-loss spectra for K_2CrO_4 exhibited almost no post L_2 edge features and this may account for the close similarity in L_3/L_2 peak ratios determined using the two background subtraction methods (Table 2).

The correlation between measured L_3/L_2 integrated-peak intensity ratios and L_3 peak positions for the Cr oxidation-state standards is shown in Fig. 10a. Measurements of the standards demonstrate that Cr oxidation states fall within well-separated regions in the correlation plot. Since the local electronic structure of the atom is responsible for the fine structure of absorption edges, other factors, in addition to valence state, influence $L_{2,3}$ fine structure, such as atom coordination, spin-orbit interactions, crystal field splitting, atomic coulomb repulsion, and exchange effects. For example, within a given oxidation

Table 2
Cr–L adsorption edge ratios

Compound	Formal valence	L_3/L_2 integrated ratio	
		Background method I (Pearson et al., 1993)	Background method 2 (Flat Two Step)
CrF_2	II	2.97 ± 0.07	2.37 ± 0.03
$CrSe$	II	2.60 ± 0.06	2.04 ± 0.02
$CrCl_3$	III	1.75 ± 0.03	1.68 ± 0.01
Cr_2O_3	III	1.81 ± 0.01	1.70 ± 0.01
$KCr(SO_4)_2 \cdot 12H_2O$	III	1.77 ± 0.02	1.60 ± 0.01
K_2CrO_4	VI	1.42 ± 0.01	1.44 ± 0.01

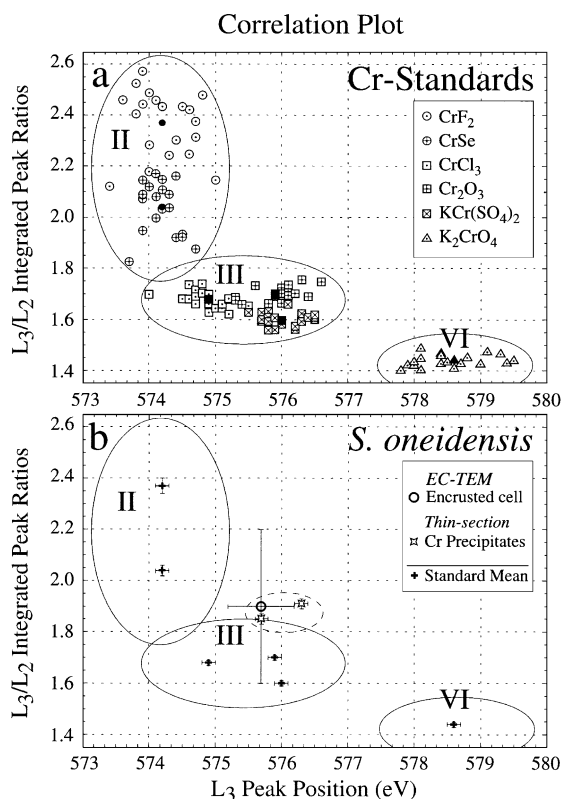


Fig. 10. The correlation between measured L_3/L_2 integrated-peak intensity ratios and L_3 peak positions for (a) the Cr oxidation-state standards, (b) bacteria and precipitates. Plotted L_3/L_2 ratios were determined using background subtraction method II. The different Cr oxidation states fall within separate regions in the plot and are labeled II, III, and VI. The solid data points represent the mean of the data for a particular Cr standard.

state in Fig. 10a, spectra for the individual standards fall within separate groupings reflecting possible differences from these factors which must be considered to correctly interpret fine structure of absorption edges. The correlation plot represents a map of the possible range in fine structure (including influences from factors other than valence state) that a particular Cr oxidation state can display.

3.5. EELS oxidation state analysis of bacterial cultures

The EELS measurements of the bacterium examined by EC-TEM and precipitates examined in thin

Table 3
Cr–L₃ (2p_{3/2}), Cr–L₂ (2p_{1/2}) adsorption-edges and L₃/L₂ integrated ratios

Specimen	CrL ₃ (2p _{3/2}) (eV)	Cr–L ₂ (2p _{1/2}) (eV)	L ₃ /L ₂ integrated ratio	
			Background method I	Background method II
Encrusted				
<i>S. oneidensis</i>	575.7 ± 0.5	584.5 ± 0.5	2.75 ± 0.30	1.90 ± 0.30
Isolated precipitates				
	575.7 ± 0.1	584.3 ± 0.1	1.72 ± 0.02	1.85 ± 0.02
	576.3 ± 0.1	584.7 ± 0.1	1.77 ± 0.02	1.91 ± 0.02

section by conventional TEM are summarized in Table 3. The error reported for the precipitates represents the standard error of the mean of 10 measurements. The error reported for the encrusted bacterium is a conservative estimate.

4. Discussion

4.1. EC-TEM techniques for microbial studies

Conventional TEM studies of microbial reduction of metals have provided important information. However, they are limited because the techniques of fixation, embedding, and microtoming, necessary to prepare thin specimens, are known to alter delicate cellular structures. Fixation and dehydration preserve some of the structure, but buffer and organic solvent washes remove extracellular polymers as well as soluble ions from extracellular and intracellular sources. Therefore, soluble, reduction intermediates can be lost. Furthermore, dehydration causes extracellular biopolymers to collapse into a filamentous, web-like network. Data on dehydration artifacts related to microorganisms has been provided by environmental scanning electron microscopy (ESEM) (Little et al., 1991). Environmental cell techniques, particularly when coupled with TEM, can be advantageous because unfixed, hydrated bacteria, still encapsulated by biopolymers, can be examined at high spatial resolution. However, damage to the unfixed, hydrated cells observed by EC-TEM occurs within minutes of electron-beam exposure during imaging. Furthermore, analysis of the L-edge spectra by EELS requires significantly higher electron doses than during imaging. In some cases, the cell boundary is ruptured

during analysis with potential mass loss. Nevertheless, if an element is detected it certainly must be associated with the bacteria, particularly when absent in the surrounding medium.

4.2. Oxidation state determination

It is difficult to explicitly deconvolve the influences on fine structure, for example, from atom coordination, spin-orbit interactions, and crystal field splitting from that of valence state. Nonetheless, the mean oxidation state of an unknown can be determined by plotting its L₃ peak position and L₃/L₂ integrated-peak intensity ratio in a correlation plot of oxidation state standards (see Fig. 10a). However, it is important that the correlation plot contain the broadest collection of standards feasible to map the full range in fine structure a particular oxidation state can display. The better these ranges are known, the more confidence can be placed in the oxidation state determination. In this regard, the data in Table 1, supplements that of Fig. 10a. Table 1 includes published L_{2,3} peak positions (absorption edge maximums) from previous EELS studies as well as core-level (or inner-shell) binding energies measured from XPS studies. In XPS, a bulk specimen is illuminated with monochromatic X-rays and the kinetic energies of ejected photoelectrons are measured. In comparison, EELS measures the energy loss of electrons that travel through a specimen. The EELS edge onset, the sudden rise in intensity preceding each of the L_{2,3} peaks, represents the ionization threshold that approximately corresponds to the inner-shell binding energy measured by XPS. The difference in chemical shift measured by EELS and XPS for oxides has been suggested to be on the order of the band-gap energy (Leapman et al., 1982), and may arise from many-body relaxation effects (more dominant in XPS) in which nearby electron orbitals are pulled towards a core hole (Egerton, 1996). Table 1 gives an indication of the range of L_{2,3} peak positions expected for each Cr oxidation state and their relative overlap (note that XPS values are reported as binding energies, not edge maxima).

The oxidation state of an unknown can be accurately determined using a correlation plot supported by a range of standards. If an unknown has components with different oxidation states, the correlation plot will reveal the predominant form. To quantify the

relative abundance of mixed oxidation states, the L_3/L_2 integrated-peak intensity of an unknown can be compared to those measured from a series of solid solutions that span a range of mixed oxidation states (van Aken et al., 1998).

The EELS measurements of the bacterium examined by EC-TEM and precipitates examined in thin section by conventional TEM are plotted in Fig. 10b. The correlation plot (Fig. 10b) indicates that Cr associated with *S. oneidensis* is most consistent with mean oxidation state of +3 or lower. Measurements of hydrated, unfixed bacteria acquired in the EC are in good agreement with the analysis of isolated precipitates measured in cross-section by conventional TEM, illustrating EELS techniques yield accurate data even under the more onerous experimental conditions of the environmental cell.

4.3. Microbial reduction

Bioaccumulation of metal precipitates by bacteria has been shown in previous SEM and TEM studies. However, only qualitative elemental identification of the precipitates associated with the bacteria was performed using EDXS (Hill and Cowley, 1986; Fude et al., 1994; Badar et al., 2000; McLean et al., 2000; Smith and Gadd, 2000; McLean and Beveridge, 2001). In none of the above mentioned studies was the oxidation state of the precipitated reduction products determined. In this work we measured the oxidation state of Cr(VI) reduction products associated *S. oneidensis*. Measurements of both the chemical shift in L_3 peak position and the ratio of L_3/L_2 integrated-peak intensities of encrusted bacteria indicate the presence of Cr in oxidation state +3 or lower. Furthermore, EELS spectra showed electron dense cell boundaries with low concentrations of Cr. However, cross-sectional TEM images of *S. oneidensis* show no evidence of intracellular precipitates. Precipitates were extracellular, in all cases, and often encrusted cells. The total mass of the encrusting Cr precipitates, in many cases, surpass the mass of the encased bacteria.

5. Summary

A method for determining oxidation state, with high spatial resolution, of metals associated with

bacteria is described. Specifically, microbial reduction of Cr(VI) by *S. oneidensis* was studied. Reduction rates suggest Cr(VI) reduction by *S. oneidensis* is mediated by living cells. Sterile medium and heat-killed or sodium-azide-treated cells did not show Cr(VI) reduction. Two distinct populations of bacteria were observed by TEM: bacteria with low image contrast and bacteria with electron-dense, high-contrast cell boundaries often encrusted with high-contrast precipitates. Chemical and oxidation state information was acquired with high spatial resolution using EELS, and showed precipitates encrusting the bacteria contained Cr of oxidation state +3 or lower. Cell boundaries were shown to be saturated with low concentrations of Cr, while no evidence of precipitates in the cytoplasm was observed. Despite the fact EELS has high sensitivity to trace elements and can determine oxidation state at subcellular scale, to our knowledge this is the first time EELS has been applied to microbial metal reduction studies. Furthermore, we demonstrate quantitative EELS oxidation state measurements can be performed using EC-TEM, which could provide data, for example, on soluble ions lost by conventional specimen preparation. To our knowledge, this is the first demonstration of EELS microanalysis by EC-TEM. Use of these techniques to study microbial reduction can reveal data on intermediate reduction products, spatial distribution of reduction products, and speciation of oxidation state necessary for determining the mechanisms(s) for microbial metal reduction or oxidation.

Acknowledgements

This work was supported by ONR program element 0602233N and ONR-ASEE Postdoctoral Fellowship Program (K. Lowe). We thank Dr. K. Neilson (University of Southern California) for kindly providing specimens of *S. oneidensis*. We thank Dr. William Straube (Geo-Centers) for fixing and embedding cultures for TEM analysis.

References

- Allen, G.C., Tucker, P.M., 1976. Multiplet splitting of X-ray photoelectron lines of chromium complexes — effect of covalency on $2p$ core level spin-orbit separation. *Inorg. Chim. Acta* 16, 41–45.

- Allen, G.C., Curtis, M.T., Hooper, A.J., Tucker, P.M., 1973. X-ray photoelectron spectroscopy of chromium–oxygen systems. *J. Chem. Soc., Dalton Trans.* 16, 1675–1683.
- Asami, K., Hashimoto, K., 1977. X-ray photoelectron-spectra of several oxides of iron and chromium. *Corros. Sci.* 17, 559–570.
- Badar, U., Ahmed, N., Beswick, A.J., Pattanapitpaisal, P., Macaskie, L.E., 2000. Reduction of chromate by microorganisms isolated from metal contaminated sites of Karachi, Pakistan. *Biotechnol. Lett.* 22, 829–836.
- Brito, F., Ascanio, J., Mateo, S., Hernández, C., Araujo, L., Gili, P., Martín-Zarza, P., Domínguez, S., Mederos, A., 1997. Equilibria of chromate(VI) species in acid medium and ab initio studies of these species. *Polyhedron* 16, 3835–3846.
- Brydson, R., Garvie, L.A.J., Craven, A.J., Sauer, H., Hofer, F., Cressey, G., 1993. $L_{2,3}$ edges of tetrahedrally coordinated d^0 transition-metal oxyanions XO_4^{n-} . *J. Phys.: Condens. Matter* 5, 9379–9392.
- Cervantes, C., 1991. Bacterial interactions with chromate. *Antonie van Leeuwenhoek* 59, 229–233.
- Cervantes, C., Campos-García, J., Devars, S., Gutiérrez-Corona, F., Loza-Tavera, H., Torres-Guzmán, J.C., Moreno-Sánchez, R., 2001. Interactions of chromium with microorganisms and plants. *FEMS Microbiol. Rev.* 25, 335–347.
- Cieslak-Golonka, M., 1995. Toxic and mutagenic effects of chromium(VI). A review. *Polyhedron* 15, 3667–3689.
- Clesceri, L.S., Greenberg, A.E., Eaton, A.D. (Eds.), 1999. *Standard Methods for the Examination of Water and Wastewater*. American Public Health Association, Washington, DC.
- Cressey, G., Henderson, C.M.B., van der Laan, G., 1993. Use of L-edge X-ray absorption spectroscopy to characterize multiple valence states of $3d$ transition metals; a new probe for mineralogical and geochemical research. *Phys. Chem. Miner.* 20, 111–119.
- Eckert, J.M., Judd, R.J., Lay, P.A., Symons, A.D., 1991. Response of chromium(V) to the diphenylcarbazine spectrophotometric method for the determination of chromium(VI). *Anal. Chem. Acta* 255, 31–33.
- Egerton, R.F., 1996. *Electron Energy-Loss Spectroscopy in the Electron Microscope*. Plenum, New York.
- Fendorf, S., Wielinga, B.W., Hansel, C.M., 2000. Chromium transformations in natural environments: the role of biological and abiological processes in chromium(VI) reduction. *Int. Geol. Rev.* 42, 691–701.
- Fink, J., Müller-Heinzerling, T., Scheerer, B., Speier, W., Hillebrecht, F.U., Fuggle, J.C., Zaanen, J., Sawatzky, G.A., 1985. $2p$ Absorption spectra of the $3d$ elements. *Phys. Rev. B* 32, 4899–4904.
- Fude, L., Harris, B., Urrutia, M.M., Beveridge, T.J., 1994. Reduction of Cr(VI) by a consortium of sulfate-reducing bacteria (SRB-III). *Appl. Environ. Microbiol.* 60, 1525–1531.
- Fukami, A., Fukushima, K., Kohyama, N., 1991. Observation technique for wet clay minerals using film-sealed environmental cell equipment attached to high-resolution electron microscope. In: Bennett, R.H., Bryant, W.R., Hulbert, M.H. (Eds.), *Microstructure of Fine-Grained Sediments from Mud to Shale*. Springer-Verlag, New York, pp. 321–331.
- Geiger, J., Schmoranz, H., 1969. Electronic and vibrational transition probabilities of isotopic hydrogen molecules H_2 , HD and D_2 based on electron energy loss spectra. *J. Mol. Spectrosc.* 32, 39–53.
- Hill, R.R.H., Cowley, H.M., 1986. Bacterial bioabsorption of chromium from industrial cooling water. *S. Afr. J. Sci.* 82, 595–596.
- Ikemoto, I., Ishii, K., Kinoshita, S., Kuroda, H., Alario-Franco, M.A., Thomas, J.M., 1976. X-ray photoelectron spectroscopic studies of CrO_2 and some related chromium compounds. *J. Solid State Chem.* 17, 425–430.
- Kendelewicz, T., Liu, P., Doyle, C.S., Brown, G.E., Nelson, E.J., Chambers, S.A., 1999. X-ray absorption and photoemission study of the absorption of aqueous Cr(VI) on single crystal hematite and magnetite surfaces. *Surf. Sci.* 424, 219–231.
- Konno, H., Tachikawa, H., Furusaki, A., Furuichi, R., 1992. Characterization of lanthanum(III) chromium(V) tetraoxide by X-ray photoelectron spectroscopy. *Anal. Sci.* 8, 641–646.
- Krishnan, K.M., 1990. Iron $L_{3,2}$ near-edge fine structure studies. *Ultramicroscopy* 32, 309–311.
- Krivanek, O.L., Paterson, J.H., 1990. ELNES of $3d$ transition-metal oxides: I. Variations across the periodic table. *Ultramicroscopy* 32, 313–318.
- Leapman, R.D., Grunes, L.A., 1980. Anomalous L_3/L_2 white-line ratios in the $3d$ transition metals. *Phys. Rev. Lett.* 45, 397–401.
- Leapman, R.D., Sun, S., 1995. Cryo-electron energy loss spectroscopy: observations on vitrified hydrated specimens and radiation damage. *Ultramicroscopy* 59, 71–79.
- Leapman, R.D., Grunes, L.A., Fejes, P.L., 1982. Study of the L_{23} edges in the $3d$ transition metals and their oxides by electron-energy-loss spectroscopy with comparisons to theory. *Phys. Rev. B* 26, 614–635.
- Lee, J.V., Gibson, D.M., Shewan, J.M., 1977. A numerical taxonomic study of some *Pseudomonas*-like marine bacteria. *J. Gen. Microbiol.* 98, 439–451.
- Little, B.J., Wagner, P., Ray, R., Pope, R., Scheetz, R., 1991. Biofilms — an ESEM evaluation of artifacts introduced during SEM preparation. *J. Ind. Microbiol.* 8, 213–221.
- Llyod, J.R., Macaskie, L.E., 1996. A novel phosphorimager-based technique for monitoring the microbial reduction of technetium. *Appl. Environ. Microbiol.* 62, 578–582.
- Lovley, D.R., 1993. Dissimilatory metal reduction. *Annu. Rev. Microbiol.* 47, 263–290.
- Lovley, D.R., Phillips, E.J.P., Gorby, Y.A., Landa, E.R., 1991. Microbial reduction of uranium. *Nature* 350, 413–416.
- Lytte, C.M., Lytle, F.W., Yang, N., Qian, J.H., Hansen, D., Zayed, A., Terry, N., 1998. Reduction of Cr(VI) to Cr(III) by wetland plants: potential for in situ heavy metal detoxification. *Environ. Sci. Technol.* 32, 3087–3093.
- MacDonell, M.T., Colwell, R.R., 1985. Phylogeny of the *Vibrionaceae*, and recommendation for two new genera, *Listonella* and *Shewanella*. *Syst. Appl. Microbiol.* 6, 171–182.
- McLean, J., Beveridge, T.J., 2001. Chromate reduction by a *Pseudomonas* isolated from a site contaminated with chromated copper arsenate. *Appl. Environ. Microbiol.* 67, 1076–1084.
- McLean, J.S., Beveridge, T.J., Phipps, D., 2000. Isolation and characterization of a chromium-reducing bacterium from a chromated copper arsenate contaminated site. *Environ. Microbiol.* 2, 611–619.

- Moffat, T.P., Latanision, R.M., Ruf, R.R., 1995. An X-ray photoelectron spectroscopy study of chromium-metalloid alloys-III. *Electrochim. Acta* 40, 1723–1734.
- Myers, C.R., Nealson, K.H., 1988a. Bacterial manganese reduction and growth with manganese oxide as the sole electron-acceptor. *Science* 240, 1319–1321.
- Myers, C.R., Nealson, K.H., 1988b. Microbial reduction of manganese oxides: interactions with iron and sulfur. *Geochim. Cosmochim. Acta* 52, 2727–2732.
- Myers, C.R., Carstens, B.P., Antholine, W.E., Myers, J.M., 2000. Chromium(VI) reductase activity is associated with the cytoplasmic membrane of anaerobically grown *Shewanella putrefaciens* MR-1. *J. Appl. Microbiol.* 88, 98–106.
- Paterson, J.H., Krivanek, O.L., 1990. ELNES of 3d transition-metal oxides: II. Variations with oxidation-state and crystal-structure. *Ultramicroscopy* 32, 319–325.
- Pearson, D.H., Ahn, C.C., Fultz, B., 1993. White lines and *d*-electron occupancies for the 3d and 4d transition metals. *Phys. Rev. B* 47, 8471–8478.
- Smith, W.L., Gadd, G.M., 2000. Reduction and precipitation of chromate by mixed culture sulphate-reducing bacterial biofilms. *J. Appl. Microbiol.* 88, 983–991.
- Spurr, A.R., 1969. A low-viscosity epoxy resin embedding medium for electron microscopy. *J. Ultrastruct. Res.* 26, 31.
- Suzuki, T., Miyata, N., Horitsu, H., Kawai, K., Takamizawa, K., Tai, Y., Okazaki, M., 1992. NAD(P)-Dependent chromium(VI) reductase of *Pseudomonas ambigua* G-1: a Cr(V) intermediate is formed during the reduction of Cr(VI) to Cr(III). *J. Bacteriol.* 174, 5340–5345.
- van Aken, P.A., Liebscher, B., Styrsa, V.J., 1998. Quantitative determination of iron oxidation states in minerals using Fe L_{2,3}-edge electron energy-loss near-edge structure spectroscopy. *Phys. Chem. Miner.* 25, 323–327.
- Venkateswaran, K., Moser, D.P., Dollhopf, M.E., Lies, D.P., Saffarini, D.A., MacGregor, B.J., Ringelberg, D.B., White, D.C., Nishijima, M., Sano, H., Burghardt, J., Stackebrandt, E., Nealson, K.H., 1999. Polyphasic taxonomy of the genus *Shewanella* and description of *Shewanella oneidensis* sp. nov. *Int. J. Syst. Bacteriol.* 49, 705–724.
- Wang, Y., 2000. Microbial reduction of chromate. In: Lovley, D.R. (Ed.), *Environmental Microbe–Metal Interactions*. ASM Press, Washington, DC, pp. 225–235.
- Wang, Z.L., Bentley, J., Evans, N.D., 1999. Mapping the valence states of transition-metal elements using energy-filtered transmission electron microscopy. *J. Phys. Chem. B* 103, 751–753.
- Wang, Z.L., Bentley, J., Evans, N.D., 2000. Valence state mapping of cobalt and manganese using near-edge fine structures. *Micron* 31, 355–362.
- Zaanen, J., Sawatzky, G.A., 1986. Strong interference between decay channels and valence-electron rearrangements in core-hole spectroscopy. *Phys. Rev. B* 33, 8074–8083.
- Zaanen, J., Sawatzky, G.A., Fink, J., Speier, W., Fuggle, J.C., 1985. L_{2,3} absorption-spectra of the lighter 3d transition-metals. *Phys. Rev. B* 32, 4905–4913.